Spectral encoding of x-ray/optical relative delay

Mina R. Bionta,[1,*] H. T. Lemke,[1] J. P. Cryan,[1,2,3] J. M. Glownia,[1,2,4] C. Bostedt,[1] M. Cammarata,[1] J.-C. Castagna,[1] Y. Ding,[1] D. M. Fritz,[1] A. R. Fry,[1] J. Krzywinski,[1] M. Messerschmidt,[1] S. Schorb,[1] M. L. Swiggers,[1] and R. N. Coffee[1]

[1]*The Linac Coherent Light Source, SLAC National Accelerator Laboratory, 2575 Sand Hill Road, Menlo Park, CA 94025, USA*

[2]*The PULSE Institute for Ultrafast Energy Science, SLAC National Accelerator Laboratory, 2575 Sand Hill Road, Menlo Park, CA 94025, USA*

[3]*Department of Physics, Stanford University, Stanford, CA 94305, USA*

[4]*Department of Applied Physics, Stanford University, Stanford, CA 94305, USA*

**mbionta@slac.stanford.edu*

Abstract: We present a new technique for measuring the relative delay between a soft x-ray FEL pulse and an optical laser that indicates a sub 25 fs RMS measurement error. An ultra-short x-ray pulse photo-ionizes a semiconductor (Si_3N_4) membrane and changes the optical transmission. An optical continuum pulse with a temporally chirped bandwidth spanning 630 nm – 710 nm interacts with the membrane such that the timing of the x-ray pulse can be determined from the onset of the spectral modulation of the transmitted optical pulse. This experiment demonstrates a nearly *in situ* single-shot measurement of the x-ray pulse arrival time relative to the ultra-short optical pulse.

OCIS codes: (120.4825) Optical time domain reflectometry; (310.6845) Thin film devices and applications; (320.2250) Femtosecond phenomena; (320.7100) Ultrafast measurements; (320.7130) Ultrafast processes in condensed matter, including semiconductors; (340.7480) X-rays, soft x-rays, extreme ultraviolet (EUV).

References and links

1. B. Steffen, V. Arsov, G. Berden, W. A. Gillespie, S. P. Jamison, A. M. MacLeod, A. F. G. van der Meer, P. J. Phillips, H. Schlarb, B. Schmidt, and P. Schmüser, "Electro-optic time profile monitors for femtosecond electron bunches at the soft x-ray free-electron laser FLASH," Phys. Rev. ST Accel. Beams **12**(3), 032802 (2009).
2. M. Krikunova, T. Maltezopoulos, A. Azima, M. Schlie, U. Frühling, H. Redlin, R. Kalms, S. Cunovic, N. M. Kabachnik, M. Wieland, and M. Drescher, "Time-resolved ion spectrometry on xenon with the jitter-compensated soft x-ray pulses of a free-electron laser," New J. Phys. **11**(12), 123019 (2009).
3. A. Azima, S. Düsterer, P. Radcliffe, H. Redlin, N. Stojanovic, W. Li, H. Schlarb, J. Feldhaus, D. Cubaynes, M. Meyer, J. Dardis, P. Hayden, P. Hough, V. Richardson, E. T. Kennedy, and J. T. Costello, "Time-resolved pump-probe experiments beyond the jitter limitations at FLASH," Appl. Phys. Lett. **94**(14), 144102 (2009).
4. A. L. Cavalieri, D. M. Fritz, S. H. Lee, P. H. Bucksbaum, D. A. Reis, J. Rudati, D. M. Mills, P. H. Fuoss, G. B. Stephenson, C. C. Kao, D. P. Siddons, D. P. Lowney, A. G. Macphee, D. Weinstein, R. W. Falcone, R. Pahl, J. Als-Nielsen, C. Blome, S. Düsterer, R. Ischebeck, H. Schlarb, H. Schulte-Schrepping, Th. Tschentscher, J. Schneider, O. Hignette, F. Sette, K. Sokolowski-Tinten, H. N. Chapman, R. W. Lee, T. N. Hansen, O. Synnergren, J. Larsson, S. Techert, J. Sheppard, J. S. Wark, M. Bergh, C. Caleman, G. Huldt, D. van der Spoel, N. Timneanu, J. Hajdu, R. A. Akre, E. Bong, P. Emma, P. Krejcik, J. Arthur, S. Brennan, K. J. Gaffney, A. M. Lindenberg, K. Luening, and J. B. Hastings, "Clocking femtosecond X rays," Phys. Rev. Lett. **94**(11), 114801 (2005).
5. P. Johnsson, A. Rouzée, W. Siu, Y. Huismans, F. Lépine, T. Marchenko, S. Düsterer, F. Tavella, N. Stojanovic, A. Azima, R. Treusch, M. F. Kling, and M. J. J. Vrakking, "Field-free molecular alignment probed by the free electron laser in Hamburg (FLASH)," J. Phys. At. Mol. Opt. Phys. **42**(13), 134017 (2009).
6. C. Gahl, A. Azima, M. Beye, M. Deppe, K. Döbrich, U. Hasslinger, F. Hennies, A. Melnikov, M. Nagasono, A. Pietzsch, M. Wolf, W. Wurth, and A. Föhlisch, "A femtosecond X-ray/optical cross-correlator," Nat. Photonics **2**(3), 165–169 (2008).
7. P. Radcliffe, S. Düsterer, A. Azima, H. Redlin, J. Feldhaus, J. Dardis, K. Kavanagh, H. Luna, J. Pedregosa Gutierrez, P. Yeates, E. T. Kennedy, J. T. Costello, A. Delserieys, C. L. S. Lewis, R. Taïeb, A. Maquet, D. Cubaynes, and M. Meyer, "Single-shot characterization of independent femtosecond extreme ultraviolet free electron and infrared laser pulses," Appl. Phys. Lett. **90**(13), 131108 (2007).

#153789 - $15.00 USD Received 1 Sep 2011; revised 5 Oct 2011; accepted 6 Oct 2011; published 20 Oct 2011

8. J. M. Glownia, J. Cryan, J. Andreasson, A. Belkacem, N. Berrah, C. I. Blaga, C. Bostedt, J. Bozek, L. F. DiMauro, L. Fang, J. Frisch, O. Gessner, M. Gühr, J. Hajdu, M. P. Hertlein, M. Hoener, G. Huang, O. Kornilov, J. P. Marangos, A. M. March, B. K. McFarland, H. Merdji, V. S. Petrovic, C. Raman, D. Ray, D. A. Reis, M. Trigo, J. L. White, W. White, R. Wilcox, L. Young, R. N. Coffee, and P. H. Bucksbaum, "Time-resolved pump-probe experiments at the LCLS," Opt. Express **18**(17), 17620–17630 (2010).
9. P. Emma, R. Akre, J. Arthur, R. Bionta, C. Bostedt, J. Bozek, A. Brachmann, P. Bucksbaum, R. Coffee, F.-J. Decker, Y. Ding, D. Dowell, S. Edstrom, A. Fisher, J. Frisch, S. Gilevich, J. Hastings, G. Hays, Ph. Hering, Z. Huang, R. Iverson, H. Loos, M. Messerschmidt, A. Miahnahri, S. Moeller, H.-D. Nuhn, G. Pile, D. Ratner, J. Rzepiela, D. Schultz, T. Smith, P. Stefan, H. Tompkins, J. Turner, J. Welch, W. White, J. Wu, G. Yocky, and J. Galayda, "First lasing and operation of an angstrom-wavelength free-electron laser," Nat. Photonics **4**(9), 641–647 (2010).
10. S. Düsterer, P. Radcliffe, C. Bostedt, J. Bozek, A. L. Cavalieri, R. Coffee, J. T. Costello, D. Cubaynes, L. F. DiMauro, Y. Ding, G. Doumy, F. Grüner, W. Helml, W. Schweinberger, R. Kienberger, A. R. Maier, M. Messerschmidt, V. Richardson, C. Roedig, T. Tschentscher, and M. Meyer, "Femtosecond X-ray Pulse Length Characterization at the LCLS Free Electron Laser," New J. Phys. (to be published).
11. M. Trigo, J. Chen, V. H. Vishwanath, Y. M. Sheu, T. Graber, R. Henning, and D. Reis, "Imaging nonequilibrium atomic vibrations with x-ray diffuse scattering," Phys. Rev. B **82**(23), 235205 (2010).
12. D. M. Fritz, D. A. Reis, B. Adams, R. A. Akre, J. Arthur, C. Blome, P. H. Bucksbaum, A. L. Cavalieri, S. Engemann, S. Fahy, R. W. Falcone, P. H. Fuoss, K. J. Gaffney, M. J. George, J. Hajdu, M. P. Hertlein, P. B. Hillyard, M. Horn-von Hoegen, M. Kammler, J. Kaspar, R. Kienberger, P. Krejcik, S. H. Lee, A. M. Lindenberg, B. McFarland, D. Meyer, T. Montagne, É. D. Murray, A. J. Nelson, M. Nicoul, R. Pahl, J. Rudati, H. Schlarb, D. P. Siddons, K. Sokolowski-Tinten, Th. Tschentscher, D. von der Linde, and J. B. Hastings, "Ultrafast Bond Softening in Bismuth: Mapping a Solid's Interatomic Potential with X-rays," Science **315**(5812), 633–636 (2007).
13. J. P. Cryan, J. M. Glownia, J. Andreasson, A. Belkacem, N. Berrah, C. I. Blaga, C. Bostedt, J. Bozek, C. Buth, L. F. DiMauro, L. Fang, O. Gessner, M. Guehr, J. Hajdu, M. P. Hertlein, M. Hoener, O. Kornilov, J. P. Marangos, A. M. March, B. K. McFarland, H. Merdji, V. S. Petrović, C. Raman, D. Ray, D. Reis, F. Tarantelli, M. Trigo, J. L. White, W. White, L. Young, P. H. Bucksbaum, and R. N. Coffee, "Auger Electron Angular Distribution of Double Core-Hole States in the Molecular Reference Frame," Phys. Rev. Lett. **105**(8), 083004 (2010).
14. A. Brachmann, C. Bostedt, J. Bozek, R. Coffee, F.-J. Decker, Y. Ding, D. Dowell, P. Emma, J. Frisch, S. Gilevich, G. Haller, G. Hays, Ph. Hering, B. Hill, Z. Huang, R. Iverson, E. Kanter, B. Kraessig, H. Loos, A. Miahnahri, H.-D. Nuhn, A. Perazzo, M. Petree, D. Ratner, R. Santra, T. Smith, S. Southworth, J. Turner, J. Welch, W. White, J. Wu, L. Young, J. M. Byrd, G. Huang, and R. Wilcox, "Femtosecond operation of the LCLS for user experiments" Stanford No. SLAC-PUB-14234 (2010), *http://www.slac.stanford.edu/cgi-wrap/getdoc/slac-pub-14234.pdf*.
15. C. Buth, R. Santra, and L. Young, "Electromagnetically Induced Transparency for X Rays," Phys. Rev. Lett. **98**(25), 253001 (2007).
16. T. E. Glover, M. P. Hertlein, S. H. Southworth, T. K. Allison, J. van Tilborg, E. P. Kanter, B. Krässig, H. R. Varma, B. Rude, R. Santra, A. Belkacem, and L. Young, "Controlling X-rays with light," Nat. Phys. **6**(1), 69–74 (2009).
17. M. P. Hertlein, T. E. Glover, T. K. Allison, J. van Tilborg, B. S. Rude, A. Belkacem, S. H. Southworth, E. P. Kanter, B. Krässig, H. R. Varma, R. Santra, and L. Young, "X-ray absorption in neon modulated by a strong laser pulse," J. Phys.: Conf. Ser. **194**(3), 032011 (2009).
18. H. R. Varma, L. Pan, D. R. Beck, and R. Santra, "X-ray-absorption near-edge structure of laser-dressed neon," Phys. Rev. A **78**(6), 065401 (2008).
19. R. N. Coffee, L. Fang, and G. N. Gibson, "Light-induced potentials ignite dissociation of N_2^{2+}," Phys. Rev. A **73**(4), 043417 (2006).
20. A. Zavriyev, P. H. Bucksbaum, H. G. Muller, and D. W. Schumacher, "Ionization and dissociation of H_2 in intense laser fields at 1.064 μm, 532 nm, and 355 nm," Phys. Rev. A **42**(9), 5500–5513 (1990).
21. F. Tavella, N. Stojanovic, G. Geloni, and M. Gensch, "Few-femtosecond timing at fourth-generation X-ray light sources," Nat. Photonics **5**(3), 162–165 (2011).
22. L. R. Rabiner and B. Gold, *Theory and Application of Digital Signal Processing* (Prentice-Hall, 1975).
23. S. M. Sze and K. K. Ng, *Physics of Semiconductor Devices* (John Wiley & Sons, Inc., 2007).

1. Introduction

Advances in optical/x-ray cross-correlation techniques are critical to the developing field of pump-probe spectroscopy at short-wavelength sources such as the xuv free-electron laser in Hamburg (FLASH) [1–7] and the Linac Coherent Light Source (LCLS) at the SLAC National Accelerator Laboratory (SLAC) [8–13]. Relative timing between independent lasers is fundamental to time resolved x-ray pump-probe spectroscopy. In typical experiments, an independent optical pulse pumps the system into a particular state and an ultrashort x-ray pulse probes the resulting excitation. Alternatively, the x-rays pump a sample while the

#153789 - $15.00 USD Received 1 Sep 2011; revised 5 Oct 2011; accepted 6 Oct 2011; published 20 Oct 2011

optical probes the state. In either case, the time-resolution of the results depends critically on a precise knowledge of the x-ray arrival time relative to the optical pulse. There are two complementary ways to approach this problem: improved synchronization and high-resolution single-shot cross-correlation measurements.

At the LCLS, the primary emphasis has been on measurement rather than synchronization, due to the sources of jitter particular to this system. The injection of electrons into the SLAC accelerator is locked to a stable 2856 MHz frequency reference. Amplitude and phase fluctuations in the klystrons that drive the linac for electron acceleration produce time fluctuations through energy-to-time coupling in the electron bunch compressors. This time jitter can be measured to an accuracy of ~10 fs by comparing electron bunch arrival time in a tuned RF cavity with the facility RF reference [14]. In addition, feedback electronics and bandwidth limiting actuators in the mode-locked lasers control the quality of the laser-to-RF locking to the ~30 fs level. Planned noise reduction in the electronics and improved locking algorithms may improve this synchronization, but only to the ~20 fs level. Beyond electronics, there are variations in the ~10 meters of optical path between the RF-locked oscillators and the experimental end-stations. With all sources of relative jitter and drift, the timing of the optical to x-rays has yet to achieve sub-100 fs root mean squared (RMS) synchronization.

There are several techniques being developed to directly measure the arrival time of the FEL x-ray pulses relative to the optical laser pulses. Photoelectron streaking, chirped-pulse laser assisted Auger decay (CPLAAD), and laser-induced transparency are based on atomic response to an optical field. Streaking and CPLAAD have strict requirements for x-ray photon energy, primary electron spectrometer resolution, and optical photon energy [3,7,10], making its implementation cumbersome. Laser induced transparency is a fundamentally resonant x-ray process, and is therefore not well matched for a tunable x-ray source [15–18]. Laser-induced molecular dissociation is a commonly used method for finding initial temporal overlap [5,8,13,19,20]. This molecular response is fundamentally limited by the vibrational time scale of the molecule.

Condensed-phase material response to the x-rays is a more robust alternative than gas-phase molecular and atomic response, with an appreciable single-shot signal [6,11]. In recent, cross-correlation between FEL generated terahertz and optical pulses yielded an accuracy of ~7 fs RMS [21]. This experiment used terahertz generated far upstream of the experiment in a geometry that is difficult to implement at the LCLS facility. Recently at the LCLS, a crossed-beam reflective geometry was used to cross-correlate the x-ray pulse with the optical pulse. This reflectivity based measurement, pioneered at FLASH [2,6], has a temporal resolution limited by the detector imaging and the optical pulse duration at the sample. Following the success of this technique, our goal has been to develop a similar technique that would avoid these limits on resolution, avoid surface quality requirements in reflective geometry and improve the accuracy of correlating x-ray and optical pulses to better than ~50 fs RMS.

Our newly developed scheme is based a common technique known as spectral encoding. In spectral encoding, a broadband laser pulse is chirped such that the different frequency components of the optical pulse arrive at the interaction point at different times. A nearly linear chirp in the continuum directly relates arrival time to frequency. A chirped continuum pulse encodes the relative x-ray/optical delay via the x-ray induced carrier dynamics in a semiconductor membrane. The temporal modulation, e.g. time-domain step-function, is due to the x-ray induced change in the free-carriers of the semiconductor [6,11]. In this case, amplitude modulation, e.g. step-function, applied in the time-domain is linearly mapped into spectrum. The rising edge of the temporal modulation produced by the x-ray interaction then manifests as a rising edge in the transmitted spectrum.

The fundamental limit for spectral encoding is the inverse of the effective spectral bandwidth convolved with the spectrometer resolution and the timescale of the physical process. Broadband continuum generation in sapphire is a common technique for white-light

#153789 - $15.00 USD Received 1 Sep 2011; revised 5 Oct 2011; accepted 6 Oct 2011; published 20 Oct 2011

continuum generation spanning the entire visible spectrum. Furthermore, commercially broadband spectrometers also span the visible spectrum with sub-1 nm resolution. Spectral encoding provides a method for determining x-ray/optical delay, measured in transmission, with a sub-25 fs RMS error in locating the rising edge that indicates the encoded delay.

2. Experiment

In this experiment, an x-ray pump pulse and a continuum probe pulse were transmitted through a 500 nm membrane of Si_3N_4. The continuum spanned ~80 nm of bandwidth and was chirped to an overall time envelope of ~3 ps. The x-ray pulses created free carriers via the photoionization of core electrons, which altered the optical properties of the Si_3N_4. The chirped continuum pulse then probed the transiently changing optical refractive index. These transient changes were encoded in the transmitted probe spectrum and measured in a spectrometer.

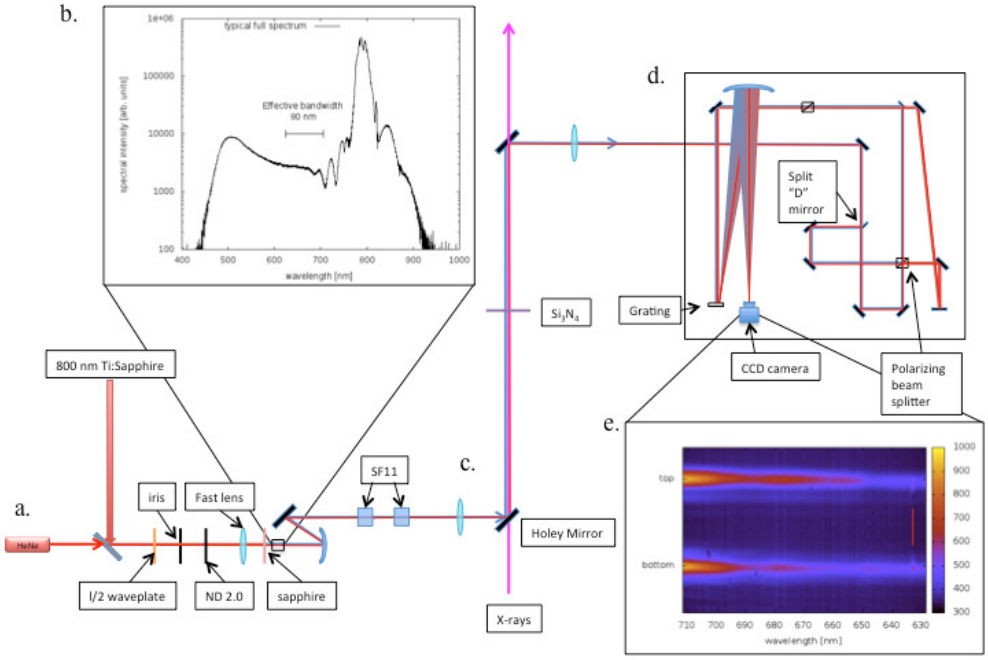

Fig. 1. (a) 100 nm of continuum was generated by focusing 800 nm Ti:Sapphire pulses into 1 mm thick *C*-plane cut sapphire. A reference HeNe was co-propagated with the 800 nm light. The continuum spectrum is shown in the inset (b). The spectrometer limited the effective bandwidth to a 620 – 700 nm smooth region that was used in this experiment. The pulses were chirped to 3 ps with 2 inches of SF11 glass. (c) The continuum then probed the Si_3N_4 membrane. The x-rays changed the index in the membrane thus changing the spectral transmission of the probe (d). Two equivalent spectra were separated into two distinct stripes as shown in the inset (e). The reference HeNe spectral line is seen on the right side of this image.

A 50 fs Ti:Sapphire laser pulse with a pulse energy of ~1 μJ and central wavelength 800 nm generated continuum in a 1 mm thick, C-cut sapphire plate as shown in Fig. 1a. The observed continuum spanned 500 nm – 900 nm, substantially overfilling the 80 nm bandwidth of the spectrometer. We directly measured the spectral resolution of the spectrometer to be ~0.8 nm. Figure 1b shows a representation of the recorded spectrum where the spectral region indicated by tick-marks was selected by the spectrometer because it was the least structured. The resulting continuum was chirped with 50 mm of SF11 glass before combining with the x-ray pulse as shown in Fig. 1a.

#153789 - $15.00 USD Received 1 Sep 2011; revised 5 Oct 2011; accepted 6 Oct 2011; published 20 Oct 2011

The Si_3N_4 was inserted into the intermediate field of the x-rays to produce an estimated ~500 μm x-ray spot ($1/e^2$) at the interaction. We used an x-ray fluence of roughly 3e12 photons/pulse in a 0.5 mm diameter spot. Linear absorption in Si_3N_4 allows an estimate of the induced free-carrier density. At 1 keV, the mass absorption of 500 nm Si_3N_4 is 2.33% for a total of ~7.3e10 absorption events. This corresponds to an initial creation of ~7e17 cc^{-1} core-ionized sites. The continuum pulse was brought into co-propagation with the x-rays by centering the beam on a mirror with a 2 mm hole as is typical in x-ray/optical experiments at the LCLS [5,8,10,11,13] (see Fig. 1c). The continuum pulse then came to a tight focus, < 100 μm, at the interaction point. The transmitted continuum light was then separated from the outgoing x-ray beam with a second mirror with a hole and re-collimated.

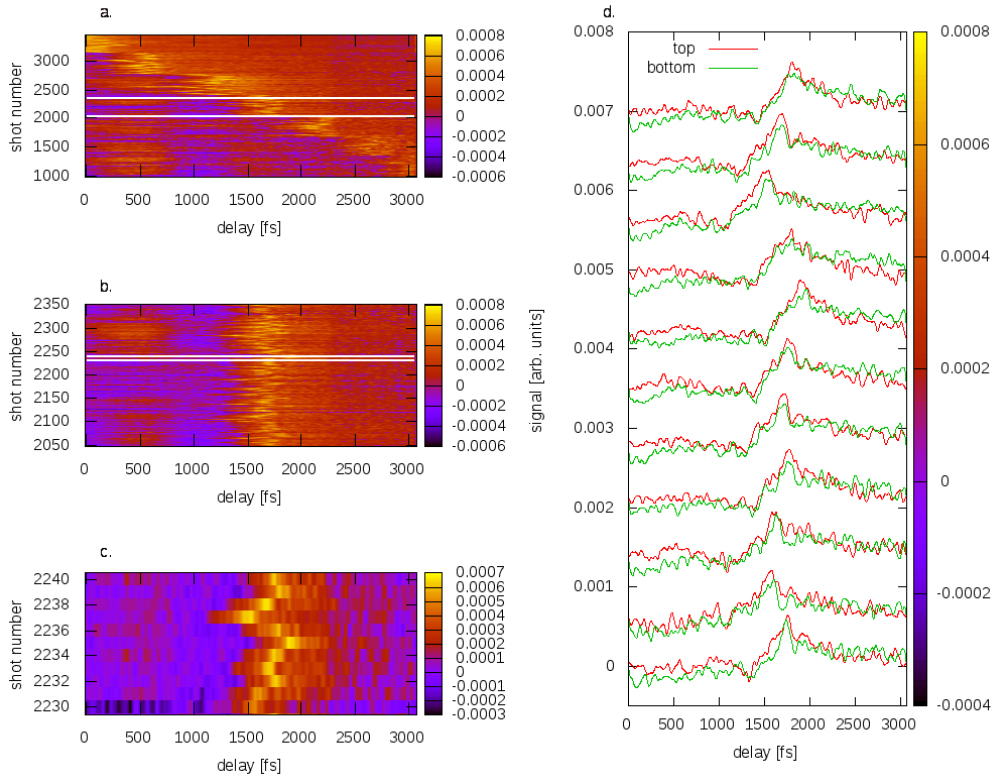

Fig. 2. Panel (a) shows the transmitted single-shot spectra, stacked so that the abscissa and ordinate correspond to the spectrum and shot-number respectively. The delay between the x-rays and the laser was scanned in 500 fs steps, twice the full width at half maximum (FWHM) natural jitter of the FEL [8]. Panels (b) and (c) incrementally zoom as indicted by the white lines in previous panels. Panel (d) shows lineouts of panel (c) shots, but for both of the correlated signal traces, top = t_1 and bottom = t_2.

The signal pulse was divided into two arms in the spectrometer using a polarizing beam splitter oriented at 45 degrees to the linear polarization of the continuum. By introducing a slight relative tilt between the two polarizations, the equivalent spectra were separated into two vertically displaced spectra in the spectrometer (see Fig. 1e). By comparing two equivalent spectra, we test our ability to locate the onset of x-ray induced refractive index change. This is similar in principle to spreading the signal in the non-dispersive dimension and comparing different regions of interest. However, focusing the spectra into two intense stripes raises the signal well above the shot-noise.

#153789 - $15.00 USD Received 1 Sep 2011; revised 5 Oct 2011; accepted 6 Oct 2011; published 20 Oct 2011

The spectrometer used a low groove density grating (150 lines/mm) such that the 6 mm horizontal dimension of the 1024 x 1024 pixel CCD array used as the detector corresponded to ~80 nm acceptance. The collimated input filled roughly 9 mm of the grating. After the grating, the dispersed spectra were focused onto a fast readout CCD camera using a 500 mm spherical mirror for an overall f/55 imaging. The spectrometer had a measured resolution of 2 nm, determined by the apparent spectral width of a co-propagated reference 633nm HeNe laser (see Fig. 1d-e).

The delay between the x-rays and the laser was scanned in 500 fs steps as shown in Fig. 2a. where the abscissa and ordinate correspond to spectrum and shot-number respectively. The delay step size was chosen to be about four times the RMS natural jitter of the FEL [8]. The total temporal window was 3 ps and therefore covered about 6 delay steps for chirp calibration. Figure 2b concentrates on a single delay setting to show the ~180 fs RMS natural relative jitter between the FEL and the laser. Figures 2c shows 11 shots that are plotted also in Fig. 2d as 2-dimensional lineouts. Figure 2d compares the signals for the two spatially separated traces as discussed above, showing the correlation between two measurements of the same signal. The two traces are independently fit for their respective arrival times, t_1 and t_2.

3. Results

We experimentally measured the spectral chirp *in situ* by scanning the relative delay in 500 fs steps across the ~3 ps temporal window as shown in Fig. 2a. All shots taken at a given delay setting were averaged and the result for all delay settings were linearly fit to give a slope of m = 37.5 fs/nm +/− 1.3 fs/nm standard error. Including a quadratic term increased the standard error by more than a factor of three, indicating that the chirp is predominantly linear. To within a few percent, the start-time of the signal is therefore a linear function of wavelength, $t = m/\lambda$ where m is proportional to the Group Delay Dispersion (GDD).

In detection, the single continuum signal is converted into two equivalent spectra for each individual shot as discussed above. The two spectra shown in Fig. 1e are individually integrated along the non-dispersed dimension and then compared to their respective references. The references are built in an identical manner as the signal, but from an average of 1000 shots taken when the continuum pulse passed the interaction region more than 1 ps before x-rays had arrived. The percentage change is calculated from the relative difference, $S = 2(sig-ref)/(sig + ref)$. This is what we refer to as "signal" throughout the manuscript.

For the sake of plotting, raw signals are filtered with the Wiener filter method [22] applied to the 1024-element signal vector. This method is based on a qualitative fit to the signal + noise ($S + N$) power spectrum such that an estimate of the two contributions is represented by an analytic expression. We use an average of all shots with a delay within the 3 ps window to calculate the $S + N$ power spectrum and we assume a flat shot-noise power spectrum that dominates primarily at high spatial frequencies.

#153789 - $15.00 USD Received 1 Sep 2011; revised 5 Oct 2011; accepted 6 Oct 2011; published 20 Oct 2011

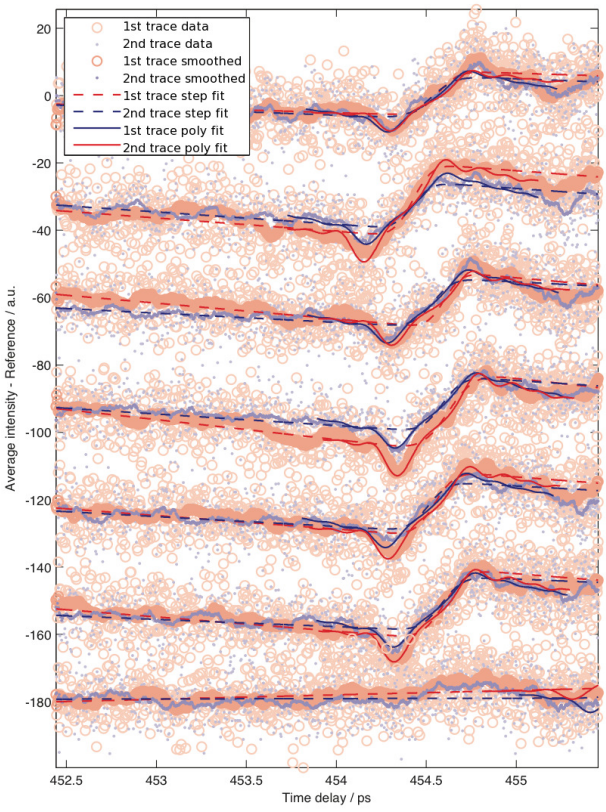

Fig. 3. Here we show an example of the two-step empirical edge-finding routine. Raw data are represented by points and circles. The two correlated traces are indicated by red and blue coloring. The raw data is shown as the open and closed circles. The dashed curve is the step function fit of step 1 in the routine as described in the text. The solid curve is the 40th order polynomial used in the second step of the fitting routine.

The timing uncertainty of the method was determined by a two-step empirical edge-finding procedure for each of the two raw signals independently, no Weiner filter was applied in the edge-finding routine. The first step of the routine is to empirically determine the instrument response. To do this, we fit the two raw traces with a step function with an underlying second order polynomial baseline. Examples of this step are shown as dashes in Fig. 3 along with the raw data as points. The resulting step-function gives us an estimate of the arrival time with which we correct for the shot-to-shot jitter. The corrected results are then averaged and fit with a 40th order polynomial (solid curves in Fig. 3), which serves as our estimate of the instrument response function. This response function is then used in the second step of the fitting routine. This curve was matched to each single-shot signal using only the baseline offset, the edge location, and the signal amplitude. Of these three parameters, we are only concerned with the edge location as it indicates the relative arrival time of the x-rays to the optical pulse.

The two extracted times for a given shot are plotted as the Cartesian coordinates of a single point (t_1,t_2) in Fig. 4b. The width of the distribution along the y = x line for a given delay setting (symbol type) indicates the natural jitter of the FEL relative to the laser. Plotted as a histogram of (t_1 + t_2)/2 in Fig. 4c, we measure an RMS width of ~180 fs, in good agreement with previous measurements [8]. The difference between the two extracted times (t_1-t_2) then gives a measure of the quality of the fitting. This difference corresponds to the width of the distribution normal to the y = x line in Fig. 4b and are plotted as a histogram in

#153789 - $15.00 USD Received 1 Sep 2011; revised 5 Oct 2011; accepted 6 Oct 2011; published 20 Oct 2011

Fig. 4a. Since the two signals are not separated until the detection stage (Fig. 1d), this measurement is not sensitive to upstream fluctuations, e.g. the shot-to-shot fluctuations in chirp of the continuum due to vibrations in the experimental area. Therefore, the RMS width of the Fig. 4a distribution only indicates our ability to locate the rising edge indicating the relative arrival time.

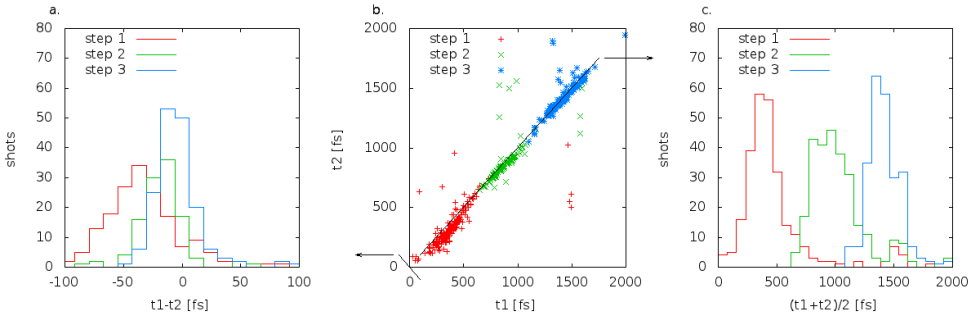

Fig. 4. Each color represents a particular laser delay set-point. Panel (a) shows the histogram of the difference of the two extracted times from the two spatially offset spectral traces. This shows that the fitting routine can locate the spectral feature indicating the time of arrival to within ~25 fs, depending on the particular delay step. Panel (b) shows the two extracted times plotted as the Cartesian coordinates of one point per shot. The different colors/points indicate each of the three delay set points that were chosen to be 500 fs apart. The coordinates show a 1:1 correlation (distributed along the $y = x$ line) since they are equivalent measurements. They differ only by the quality of the time-extraction fitting routine. The correlated times are projected along the indicated axis and plotted as indicated by arrows in Panels (a) and (c). Panel (c) shows a histogram of the average of the two measured arrival times per shot. This histogram reflects the natural FEL jitter of ~180 fs RMS relative to the optical laser.

Our ability to extract arrival times depends on the spectral intensity where the overlap signal occurs. This dependence corresponds to a reduced signal-to-noise ratio as the overlap time moves to the weaker 630 nm side of our spectrum (see Fig. 1e). For the three set-points used for this analysis, we find RMS widths of 19.4 fs, 20.2 fs, and 36.5 fs for the long, medium, and short wavelength sides of the spectrum (left, middle, right parts of the traces in Fig. 1e). Averaged over the three regions shown in Fig. 4, we locate the spectral edge indicating the x-ray arrival time to within an RMS error of 25 fs.

4. Discussion

The time resolution of a spectral-encoding technique is tied to the overall time window via the spectral chirp parameter. We control the chirp by changing the amount of glass inserted in the continuum. In this experiment, 50 mm of SF11 glass caused the 630 nm end of the spectrum to arrive about 3 ps later in time than the 710 nm end. Decreasing chirp (less glass) reduces the temporal window but improves the resolution, providing a simple way to zoom in on the temporal features of interest. Indeed, an initial setup experiment confirmed that changing the thickness of glass allowed for a variable temporal window between 500 fs and 3 ps.

The dependence of resolution on chirp comes from the time-bandwidth product of the transient signal itself—the larger the spectral-bandwidth that experiences the transient effect the higher the temporal resolution. The rising signal spans only about 6.5 nm, which corresponds to a ~150 fs blurring. Adding in quadrature the 75 fs x-ray pulse duration, the 150 fs time-bandwidth resolution, and the 0.8 nm spectral resolution gives an overall feature resolution of 174 fs. This is in reasonable agreement with the ~200 fs rising-edge width of the signal in Fig. 5.

We correlated two replica spectra to measure our confidence in locating the rising edge of the transient signal. As described above, the single-shot spectra are split into two traces on the same spectrometer and each is independently fit by a step-like response function. Figure 4b

#153789 - $15.00 USD Received 1 Sep 2011; revised 5 Oct 2011; accepted 6 Oct 2011; published 20 Oct 2011

shows a correlation plot of the two rising edges. The correlation plot is built from points defined by the Cartesian coordinates (t_1,t_2) from the two extracted edge locations. Ideally, the points would lie perfectly along the $y = x$ line since they are derived from the same transmitted spectrum. The scatter of the points away from $y = x$ is only due to the error in locating the edges t_1 and t_2. The error exhibits a normal distribution with as little as 19.5 fs RMS width. We have demonstrated that the ~200 fs rising edge, which indicates the arrival time of the x-rays relative to the continuum pulse, can be resolved to better than 25 fs RMS under our experimental conditions.

To form a qualitative model of the dynamics as plotted in Fig. 5, we solve the following system of differential equations:

$$\dot{p}(t) = f(t) - \kappa_p p(t) \tag{1}$$

$$\dot{a}(t) = \alpha p(t) - \kappa_a a(t) \tag{2}$$

$$\dot{q}(t) = \kappa_p p(t) + \kappa_a a(t) - \rho q(t) \tag{3}$$

where p indicates primary electrons, f indicates the x-ray pulse envelope, κ_p is an rate of conversion of the primary hot electrons to signal carriers, a are secondary hot electrons, α is the rate of production of secondary hot electrons, κ_a is the rate of conversion of the secondary hot electrons to signal carriers, ρ is the overall decay of signal, and q is the number of signal carriers. Fourier transforming the above set of equations and algebraically solving in Fourier space yields

$$Q = \left[\frac{\kappa_p}{(i\omega + \kappa_p)(i\omega + \rho)} + \frac{\kappa_a \alpha}{(i\omega + \kappa_p)(i\omega + \kappa_a)(i\omega + \rho)} \right] \frac{\tau}{\sqrt{2}} \exp\left(-i\omega t_0 - \frac{\tau^2 \omega^2}{4} \right), \tag{4}$$

where Q is the Fourier transform of the free carriers and τ is the width of a Gaussian x-ray pulse, and t_0 is the x-ray arrival time. This is a quasi-empirical rate equation model. Assuming the time-domain function $q(t)$ is proportional to the index change of the material, the input parameters represent the conversion of hot electrons, κ_p and κ_a from the photoionization and Auger decay rates respectively, into lower energy electrons with a roughly 10:1 conversion. The Si_3N_4 exhibits a fast recovery of about 2 ps^{-1}.

The rising and falling time constants in our signal are 200 fs and 500 fs respectively. The 630 – 710 nm (2 – 1.75 eV) optical probe lies well below the ~5 eV Si_3N_4 band gap [23]. We believe that our signal is sensitive only to the fast, ~1 ps thermalization rather than to the hundreds of picoseconds long electron-hole recombination observed in GaAs [6]. The fast 200 fs rising edge is most likely due to the prompt creation of hot electrons via core-ionization. The bi-exponential sub-picosecond decay observed in Fig. 5 indicates a more complicated electron thermalization.

#153789 - $15.00 USD Received 1 Sep 2011; revised 5 Oct 2011; accepted 6 Oct 2011; published 20 Oct 2011

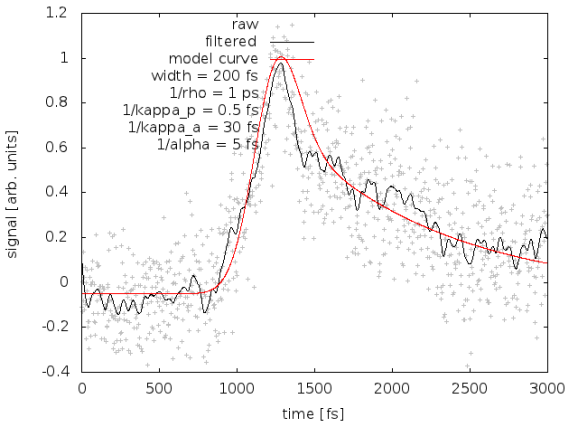

Fig. 5. Raw data filtered by a Wiener filter along with the hand fit model curve.

Localized core-ionized sites may affect the optical transmission in either of two ways: lowering the absorption gap and providing defect-mediated electron-hole recombination. As effective dopants, localized holes accumulate as the integral of the temporal profile of the x-ray pulse. These effective dopants can lower the local band-gap, shifting the absorption edge to lower frequency. This would raise both the real and imaginary parts of the refractive index of the material, increasing both the reflectance and the absorption of the material. In addition, the effective dopants can mediate electron-hole recombination. This process can substantially speed recombination and may be indicated by the apparent fast decay portion of the bi-exponential function in Fig. 5. Cascade Auger relaxation will convert the localized core-holes into partly delocalized holes in the valence band, as well as produce more hot electrons. This process could quench the effect of the dopant-induced optical response while increasing the total number of delocalized free-carriers. Ultimately, the hot electrons cool into a ~1e19/cc free-carrier density or higher depending on the temperature of the final thermalized conduction-band energy distribution. The dynamics of the free-carrier and core-hole conversion in the material makes for a complicated transient optical transmission.

5. Conclusions

The method presented in this article uses a spectrum-to-time mapping technique known as spectral encoding to measure the arrival time of an x-ray pulse relative to an optical pulse. The modulation of the optical probe is the result of the response of a Si_3N_4 membrane to x-ray laser excitation. This response produces a temporal edge-like feature in the transmission function of the membrane. Since the probe pulse encodes time-to-frequency, this transmission function is linearly mapped to a spectral transmission. Accounting for the spectrum-to-time calibration, we locate the rising edge of this transmission function with an RMS error better than 25 fs. Further investigation is required to better understand the physical processes, namely, how close the probe photon energy to the band gap influences the various time-constants.

The use of the Fast Fourier Transform (FFT) could eventually enable a real-time shot-to-shot cross-correlation. Once the parameters are found to best replicate the signal as in Fig. 5, the model curve can be used in a Wiener deconvolution routine with the original signal. The deconvolution would yield a peaked function where the peak corresponds to the “best-fit” time delay, real-time on a shot-to-shot basis.

Acknowledgments

We would like to thank, Steve Durbin, David Reis, Stephen Fahy, Martin Beye, Adi Natan, and William Schlotter for their important scientific input. We would also like to thank Jim

#153789 - $15.00 USD Received 1 Sep 2011; revised 5 Oct 2011; accepted 6 Oct 2011; published 20 Oct 2011

Turner, Rick Iverson, Paul Emma, Zhirong Huang, and the LCLS Accelerator Directorate for allowing these important Machine Development (MD) studies.

This research was carried out entirely at the Linac Coherent Light Source (LCLS) at the SLAC National Accelerator Laboratory. LCLS is an Office of Science User Facility operated for the U.S. Department of Energy Office of Science by Stanford University.

#153789 - $15.00 USD Received 1 Sep 2011; revised 5 Oct 2011; accepted 6 Oct 2011; published 20 Oct 2011